THE JOURNAL OF PHYSICAL CHEMISTRY C
A JOURNAL OF THE AMERICAN CHEMICAL SOCIETY

pubs.acs.org/JPCC

Article

Nonvolatile Electric Field Control of Magnetism in the Janus Cr_2S_2Se Monolayer

Deju Zhang, Zhe Wang, Sihang Che, Wei Ji, and Yanning Zhang*

Cite This: *J. Phys. Chem. C* 2026, 130, 4216−4222

Read Online

ACCESS | Metrics & More | Article Recommendations | Supporting Information

ABSTRACT: In the field of low-energy-consumption applications, electrical control of magnetism has attracted considerable research attention. Here, we report that the Janus Cr_2S_2Se monolayer, where Se atoms substitute the upper S layer in the Cr_2S_3 monolayer, is structural stable. We find that the Janus Cr_2S_2Se monolayer favors the ferromagnetic configuration with a high Curie temperature of 279 K, and shows semiconducting characteristics with an indirect band gap of 0.44 eV and a valley splitting of 33 meV. By constructing a van der Waals multiferroic heterostructure combined with α-In_2Se_3 monolayer, its interlayer magnetism can be switched between two types of magnetic coupling via nonvolatile manipulation of the ferroelectric polarization. Our study reveals the switchable magnetism of the Janus Cr_2S_2Se monolayer, making it promising candidates for use in next-generation low-dimensional spintronics applications.

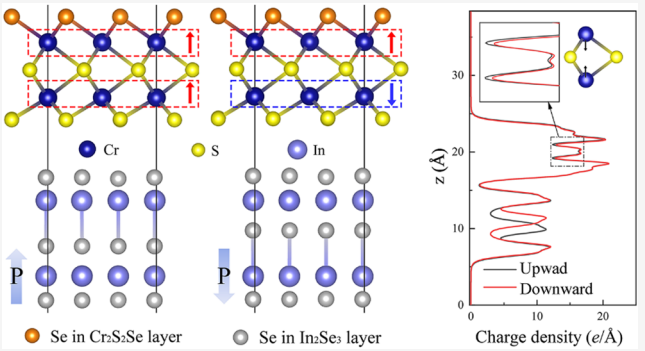

1. INTRODUCTION

Magnetoelectric multiferroic materials have garnered significant research attention, owing to their coupled ferromagnetic (FM) and ferroelectric (FE) properties, which enable electric field control of magnetism.[1,2] Among them, two-dimensional (2D) multiferroics are particularly promising for achieving further miniaturization and enhanced integration in spintronic devices.[3,4] As material dimensions are reduced to the atomic scale, however, many physical properties present in their bulk counterparts can change dramatically or even vanish.[5−7] Realizing multiferroicity in 2D materials is particularly challenging as a result of the complex interactions among charge, spin, and lattice structures.[8,9] Consequently, the search for and understanding of 2D multiferroic materials has become a forefront research area in condensed matter physics and materials science.

Both theoretical and experimental studies have made substantial progress in addressing this challenge through innovative material design strategies.[10,11] A particularly effective strategy involves constructing van der Waals (vdW) heterostructure, which offers an exciting platform to explore multitudinous properties such as 2D multiferroics.[3,4] However, a critical challenge remains in the design of materials that can serve as highly responsive components within these heterostructures. Janus structures inherently break mirror symmetry and thereby induce many interesting properties.[12−16] Over the past decades, extensive efforts have been devoted to exploring Janus materials with exotic electronic and magnetic properties, such as chromium-based halides[17,18] and dichalcogenide halides.[19] It creates opportunities for exploring multifunctional 2D materials, particularly those with electrically controllable magnetism.

In this work, we systematically investigate the structural, electronic, and magnetic properties of the Janus Cr_2S_2Se monolayer. This Janus structure is derived from the Cr_2S_3 monolayer by substituting the upper S layer with Se and exhibits high structural stability for potential experimental realization. It is found to be an indirect-band gap semiconductor exhibiting pronounced valley polarization with enhanced valley splitting. It also possesses intrinsic electric polarization and ferromagnetism with a high Curie temperature (T_C). Moreover, for the vdW multiferroic heterostructure composed of the Janus Cr_2S_2Se and α-In_2Se_3 monolayers, the interlayer magnetic coupling in the Cr_2S_2Se layer can be reversibly switched between the FM and antiferromagnetic (AFM) states by means of reversing the ferroelectric polarization direction of the α-In_2Se_3 layer. Overall, our findings identify the Janus Cr_2S_2Se monolayer as a promising candidate for realizing magnetoelectric multiferroicity in 2D heterojunctions, and the insights gained here can be extended to guide the discovery of other novel switchable 2D functional materials.

Received: November 26, 2025
Revised: February 21, 2026
Accepted: February 23, 2026
Published: March 4, 2026

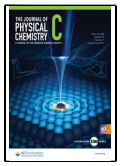

https://doi.org/10.1021/acs.jpcc.5c08067
J. Phys. Chem. C 2026, 130, 4216−4222

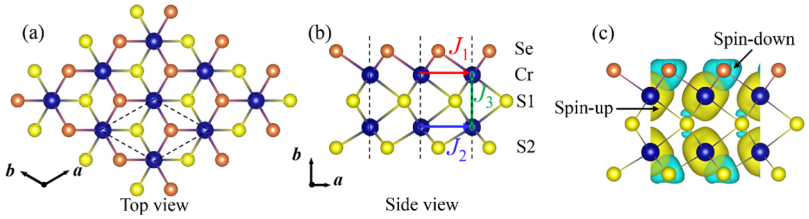

Figure 1. Crystal structure of the Janus Cr_2S_2Se monolayer shown as (a) top and (b) side views. In the schematic, Cr, S, and Se atoms are represented by blue, yellow, and orange spheres, respectively. The nearest-neighbor Cr−S/Se−Cr, Cr−S/S−Cr, and second-nearest-neighbor Cr−S/S−Cr exchange paths are represented by red, blue, and green arrows, respectively. Black dashed lines show the unit cell. (c) Spin density of the Janus Cr_2S_2Se monolayer with an isovalue of 0.07 e/Bohr^3.

2. METHODS

The first-principles calculations based on density functional theory (DFT) are performed using the Vienna *ab initio* simulation package.[20,21] The Perdew-Burke-Enzerhof functional within the generalized gradient approximation and the projector-augmented-wave method are used to describe the exchange-correlation potential.[22−24] The plane wave energy cutoff is set to 600 eV. To consider the strong correlation effect among Cr-3d electrons, we test different effective U values and adopt U = 3.0 eV, consistent with previous studies,[25−28] as shown in Figure S1 in the Supporting Information (SI). All structural relaxations are performed until the convergence criteria were met, with that for energy and atomic force set at 1×10^{-6} eV and 1×10^{-3} eV·Å^{-1}, respectively. The electronic configurations $3d^54s^1$, $3s^23p^4$, $4s^24p^4$, and $5s^25p^1$ are considered as the valence states of Cr, S, Se, and In, respectively. A vacuum spacing larger than 15 Å is added along the out-of-plane direction to eliminate interactions between periodic images. A 2 × 2 × 1 supercell with 7 × 7 × 1 k-point grid are adopted for the calculations of exchange coupling parameters and phonon spectrum, with the former evaluated using the single-point energy mapping method[29−31] and the latter obtained using the PHONOPY code and the finite displacement method.[32,33] A 11 × 11 × 1 k-point mesh is used to calculate the band structures and magnetocrystalline anisotropy energies (MAEs). For the *ab initio* molecular dynamics (AIMD) simulations, a 3 × 3 × 1 supercell is constructed, and only the Γ-point is used for Brillouin zone (BZ) sampling. The simulations were performed at 300 K for a total duration of 8 ps. Monte Carlo (MC) simulations based on the Heisenberg model are performed on a 30 × 30 × 1 supercell to determine the magnetic transition temperature.

3. RESULTS AND DISCUSSIONS

3.1. Structural Properties

The crystal structure of the Janus Cr_2S_2Se monolayer, which belongs to the $P3m1$ space group (No. 156), is obtained by substituting the upper S atoms in the Cr_2S_3 monolayer with Se atoms. As illustrated in Figure 1a,b, each primitive cell contains two nonequivalent magnetic Cr atoms, forming a honeycomb lattice in-plane and stacked perpendicularly along the z direction with a S layer in the middle. The upper Se and bottom S atoms are located at $(2/3, 1/3, h_{Se,S2})$ and the middle S atoms are coordinated at $(1/3, 2/3, h_{S1})$, respectively. To obtain lattice parameters a and b and height parameters h, both the lattice and atom coordinates are fully relaxed. The calculated lattice parameters are $a = b = 3.54$ Å, while parameters h_{Se}, h_{S1}, and h_{S2} are 0.598, 0.499, and 0.406, respectively. Notably, the lattice constant of the Janus Cr_2S_2Se monolayer is about 1.7% larger than that of the Cr_2S_3 monolayer, attributed to the larger atomic radius of Se compared to S, consistent with previous studies.[34−36]

A key question is whether this hypothetical structure is stable and is experimentally realizable. To address this, we examine the Janus Cr_2S_2Se monolayer from three complementary aspects. First, we evaluate its energetic stability by calculating the formation energy, defined as

$$E_f = (E_{mon} - 2E_{Cr} - 2E_S - E_{Se})/5 \quad (1)$$

Here, E_{mon}, E_{Cr}, E_S, and E_{Se} are the energies of the Cr_2S_2Se monolayer and chromium, sulfur, and selenium in their stable phases in ambient conditions, respectively. Encouragingly, the calculated E_f is negative, about −0.34 eV/atom, indicating that the synthesis of the Janus Cr_2S_2Se monolayer is energetically favorable and thermodynamically feasible. Experimentally, some Janus monolayers have already been successfully fabricated, such as MoSSe obtained via a controlled colloidal chemical synthesis method.[37] The techniques developed for such Janus monolayers can, in principle, be readily adapted for the preparation of Janus Cr_2S_2Se monolayer.

Second, we calculated the phonon spectrum of the Janus Cr_2S_2Se monolayer. As shown in Figure S2 in the SI, all phonon modes exhibit positive frequencies throughout the BZ, confirming the thermal dynamical stability of the structure. Finally, we perform AIMD simulations at 300 K up to 8 ps. The Janus Cr_2S_2Se monolayer retains its structural integrity without noticeable distortion during the simulation (see Figure S3 in the SI). Overall, these results demonstrate that the Janus Cr_2S_2Se monolayer possesses strong energetic, dynamic, and thermal stabilities, suggesting that its experimental realization is feasible. This stability foundation allows us to further explore its magnetic and electronic properties in the following sections.

3.2. Magnetic Properties

To identify the magnetic ground state and determine the exchange coupling between different Cr−Cr pairs in the Janus Cr_2S_2Se monolayer, we use a 2 × 2 × 1 supercell and examined four distinct magnetic configurations as shown in Figure S4 of the SI. These include the FM, the interlayer AFM (iAFM) state with all-spin-up in the upper Cr layer and all-spin-down in the lower Cr layer, and two ferrimagnetic configurations: iFM1 featuring a striped AFM in the upper Cr layer and all-spin-down in the lower layer, and iFM2, in which the upper layer has all-spin-down while the lower layer has a striped AFM pattern. We fit the exchange parameters based on the Heisenberg model as follows

$$H = H_0 - J_n \sum_{<i,j>} \vec{S_i} \cdot \vec{S_j} (n = 1,\ 2,\ 3) \quad (2)$$

Here, S_i and S_j are the spin vectors, J_1 and J_2 represent the exchange paths in the upper and lower Cr layers, and J_3 represents the interlayer exchange paths between the two Cr layers, respectively, as illustrated in Figure 1. Obviously, the positive and negative J values are the FM and AFM couplings,

https://doi.org/10.1021/acs.jpcc.5c08067
J. Phys. Chem. C 2026, 130, 4216−4222

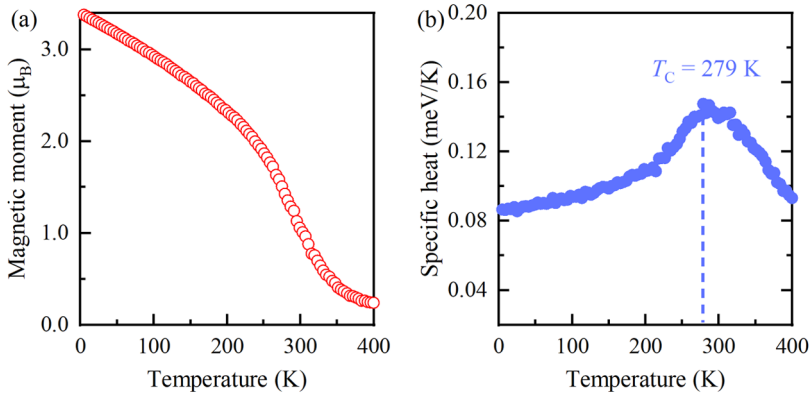

Figure 2. MC simulations of the (a) magnetic moment and (b) specific heat of the Janus Cr_2S_2Se monolayer as functions of temperature. The magnetic moment and specific heat are represented by red and blue symbols, respectively. The calculated T_C, defined as the temperature at the maximum of the specific heat, is shown in the inset.

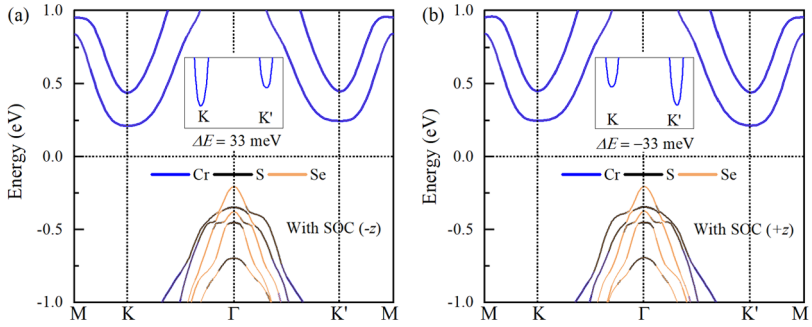

Figure 3. Projected band structures of the Janus Cr_2S_2Se monolayer considering SOC for the magnetization along the (a) $-z$ and (b) $+z$ directions. The blue, black, and orange lines represent the Cr, S, and Se states. The enlarged conduction bands around the high-symmetric k points K and K′ are in the inset.

respectively. According to the model, the energies corresponding to the four magnetic configurations are expressed as

$$E_{FM} = E_0 + (-12J_1 - 12J_2 - 4J_3)\,S^2,$$
$$E_{iFM1} = E_0 + (+4J_1 - 12J_2)\,S^2,$$
$$E_{iFM2} = E_0 + (-12J_1 + 4J_2)\,S^2,$$
$$E_{iAFM} = E_0 + (-12J_1 - 12J_2 + 4J_3)\,S^2 \quad (3)$$

From the calculated total energies of the four configurations, we find that the Janus Cr_2S_2Se monolayer has the FM ground state and the exchange parameters are J_1 = 7.02, J_2 = 8.90, and J_3 = 0.29 meV, respectively. For the magnetic ground state, the absolute magnetic moment per magnetic atom is about 3.3 μ_B, which indicates a S = 3/2 state. The strong interaction between magnetic and nonmetallic atoms induces obvious spin polarizations on S1, S2, and Se with magnetic moments of 0.2, 0.1, and 0.3 μ_B, respectively, as shown in Figure 1c. The antiparallel ordered moments give rise to a net magnetization of 3.0 μ_B per formula unit. According to the well-established Goodenough-Kanamori-Anderson rules, the nature of superexchange interactions between two magnetic atoms is primarily governed by the bond angle formed with the intervening nonmetallic atom.[38−40] When the bond angle approaches 90°, the FM coupling is typically favored, whereas an angle close to 180° generally gives rise to the AFM coupling. In the Janus Cr_2S_2Se monolayer, the Cr-X-Cr (X = S and Se) bond angles range from 75° to 96°, indicating the predominant FM superexchange interactions along these superexchange pathways. The competing AFM direct exchange is effectively suppressed, as reflected in the Bethe-Slater interaction (BSI) curve,[41−43] leading to the FM ground state and all-positive exchange parameters.

To sustain FM order in a 2D magnet at a finite temperature, a sizable magnetic anisotropy is essential. To access this property, we include spin−orbit coupling (SOC) in our calculations for different spin orientations and evaluated the MAE of the Janus Cr_2S_2Se monolayer. The uniaxial MAE is calculated from the energy difference $E_x - E_z$, where E_x and E_z are the total energies for the x and z axes, respectively. A negative (positive) MAE denotes in-plane (perpendicular) magnetic anisotropy. Our results show that the Janus Cr_2S_2Se monolayer prefers an in-plane magnetic anisotropy with a MAE of −64 μeV/Cr, which mainly comes from the Se-p_x/p_y orbital, as shown in Figure S5 of the SI.

Using the DFT-derived exchange parameters J and magnetic anisotropy constant A, we perform MC simulations based on the anisotropic Heisenberg model

$$H = -J_n \sum_{<i,j>} \vec{S_i}\cdot\vec{S_j} - \sum_i A(S_{i,z})^2 \ (n = 1,\ 2,\ 3) \quad (4)$$

to estimate the T_C of the Janus Cr_2S_2Se monolayer. Figure 2 depicts the temperature dependences of magnetic moment and specific heat, where the peak position of the specific heat corresponds to the estimated T_C. As shown in Figure 2, the Janus Cr_2S_2Se monolayer exhibits a T_C of approximately 279 K. This value is much higher than those of many 2D FM

https://doi.org/10.1021/acs.jpcc.5c08067
J. Phys. Chem. C 2026, 130, 4216−4222

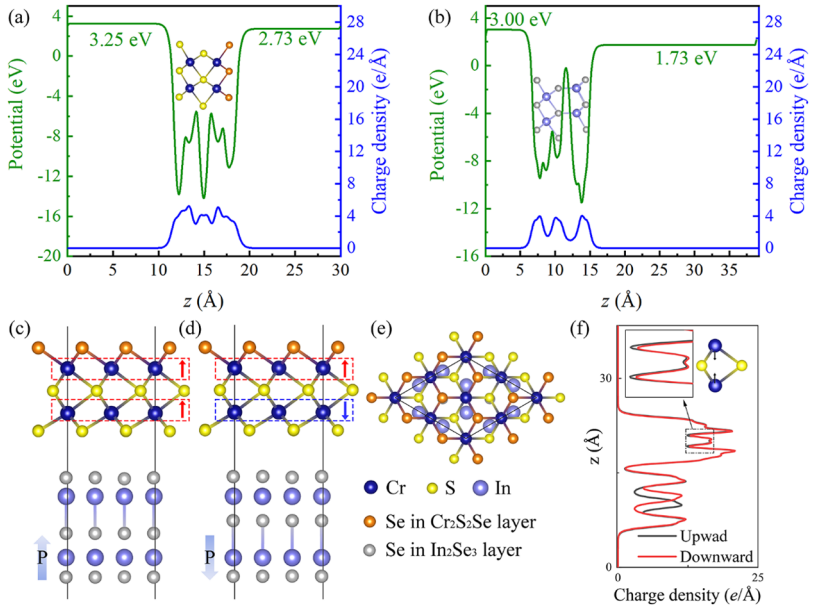

Figure 4. Electrostatic potentials and plane-average charge densities of (a) the Janus Cr_2S_2Se monolayer and (b) the In_2Se_3 monolayer. The structures of these two monolayers are inset. The schematic models of Cr_2S_2Se/In_2Se_3 heterostructure with (c) upward and (d) downward polarizations in side views and those in (e) top view, in which the top views for two directions of polarization are the same. The directions of polarizations are marked by gradual arrows, and the different directions of magnetic moments are marked by red and blue arrows. (f) In-plane average charge density of the Cr_2S_2Se/In_2Se_3 heterostructure with upward and downward polarizations. The enlarged structure of the Cr−S/S−Cr path is inset, in which the structural deformations are marked by black arrows.

materials, such as the CrI_3 monolayer (45 K)[5] and the $Cr_2Ge_2Te_6$ bilayer (28 K)[6], indicating its strong magnetic stability and promising potential for experimental verification and spintronic applications.

3.3. Electronic Properties

To elucidate the electronic properties of the Janus Cr_2S_2Se monolayer, we calculate its projected band structure and density of states (DOS), including SOC with the magnetization oriented along the $-z$ direction. As shown in Figures 3a and S6 in the SI, our results show that it is an indirect-band gap semiconductor with a band gap of 0.44 eV. The conduction band minimum (CBM) is positioned at the high-symmetric K/K′ points and is predominantly contributed by the Cr-3d orbitals, whereas the valence band maximum (VBM) appears at the Γ point and mainly originates from Se-p orbitals. Further orbital projections assign the CBM mainly to the Cr-d_z^2 orbital and the VBM to the Se-p_x orbital, as shown in Figure S7 of the SI. As a result of broken degeneracy, two energetically distinct valleys emerge at the K and K′ points. The energy of the K valley is lower than that of the K′ valley, giving rise to a valley polarization characterized by a splitting of ΔE = 33 meV. Here, ΔE is defined as $\Delta E = E_{K'} - E_K$, where $E_{K'}$ and E_K are energy levels at CBMs. For the $+z$ direction, the valley polarization is reversed and the value of ΔE becomes −33 meV, as shown in Figure 3b. It should be noted that the value of ΔE in the Janus Cr_2S_2Se monolayer is much higher than that of the Cr_2S_3 monolayer (22 meV),[34] indicating that the Janus structure enhances valley splitting and holds promise for future valleytronic and data storage applications.

For the x-magnetization, the indirect band gaps of the Janus Cr_2S_2Se monolayer become 0.50 eV. As shown in Figure S8 in the SI, the band features and orbital occupations approximately remain the same. Nevertheless, the valley polarization at K′ and K points disappears. We also calculate the spin-polarized band structure without the inclusion of SOC. As shown in Figure S8 in the SI, the indirect band gaps become 0.54 eV.

3.4. Cr_2S_2Se/In_2Se_3 Heterostructure

Both theoretical and experimental studies have demonstrated that the vdW heterostructures integrating 2D materials with diverse functionalities offer exciting platforms for realizing emergent physical phenomena.[44−46] To modulate the exotic magnetic properties of the Janus Cr_2S_2Se monolayer, it is of great interest to construct a heterostructure with the ferroelectric α-In_2Se_3 monolayer and explore the possibility of controlling its magnetism through the reversal of the electric polarization. In particular, we focus on the potential enhancement of transition temperature and valley polarization in such a heterostructure. The discussion above demonstrated that the lattice parameters of the Janus Cr_2S_2Se monolayer is about 3.54 Å, which is suitable for the typical ferroelectric materials α-In_2Se_3 monolayer. We use a 2 × 2 cell of the Janus Cr_2S_2Se monolayer and a $\sqrt{3} \times \sqrt{3}$ cell of the α-In_2Se_3 monolayer to build the vdW heterostructure, for which the lattice mismatch is only 0.2%. We first adopted the in-plane lattice constant of the $Cr_2S_2Se_2$ layer as the reference to construct the initial heterostructure, and subsequently performed structural relaxation with the out-of-plane lattice parameter fixed to obtain an equilibrium structure.[47,48] Due to the elemental substitution-induced symmetry breaking, the electrostatic potential of Janus Cr_2S_2Se monolayer is different in two sides, with a potential drop of about 0.52 eV, as shown in Figure 4a. Likewise, there is a potential difference of about 1.27 eV between two sides of the α-In_2Se_3 monolayer because of its inherent ferroelectricity, as shown in Figure 4b. The crystal structure of the Cr_2S_2Se/In_2Se_3 heterostructure in the side and top views is shown in Figure 4c−e, in which the Se atoms in Cr_2S_2Se and α-In_2Se_3 layers are distinguished by the spheres with different colors.

https://doi.org/10.1021/acs.jpcc.5c08067
J. Phys. Chem. C 2026, 130, 4216−4222

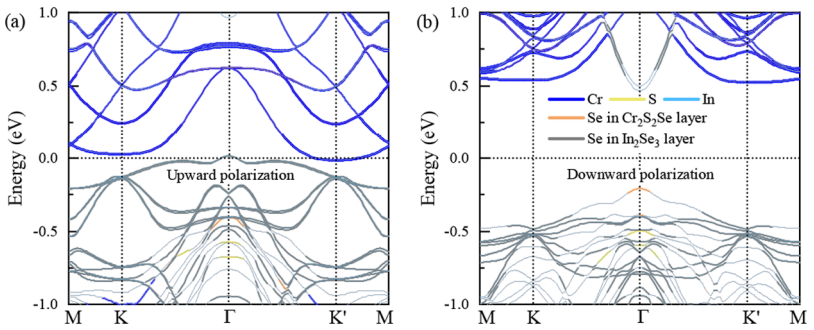

Figure 5. Projected band structures of Cr_2S_2Se/In_2Se_3 heterostructure with (a) upward and (b) downward polarizations, in which the SOC for magnetization along the $+z$ direction is considered. The blue, yellow, and cyan lines represent the Cr, S, and In states, and the orange and gray lines represent the states of Se in the Cr_2S_2Se and In_2Se_3 layer, respectively.

When the electric polarization in the In_2Se_3 layer is upward, which is parallel to the electric polarization of the Cr_2S_2Se layer, the ferromagnetism retains. As the polarization reverses, it changes the direction of inherent polarization of the Cr_2S_2Se layer. We calculate the energy difference between the FM and iAFM states in the structure of α-In_2Se_3 attached to Janus Cr_2S_2Se monolayer without relaxation to consider the effect of charge transfer, and that in the heterojunctions after removing the α-In_2Se_3 layer to consider the effect of structural deformation. With the reversal of polarization from upward to downward, charge transfer enhances the interlayer FM coupling, while structural deformation enhances the AFM interaction (Table S1 in the SI). We also calculate the charge transfer during polarization reversal for both the upward and downward polarization directions, as shown in Figure 4f. To quantify the charge transfer, we integrate the charge density within the Cr_2S_2Se layer. Our results indicate that when the polarization is reversed downward, more charge accumulates in the Cr_2S_2Se layer, with an increase of 0.014 e compared to the upward polarization. The Cr−Cr bond corresponding to J_3 is shortened by 0.6 Å. The increased charge density likely enhances FM coupling through double-exchange effects,[49] while the shortening of bond lengths suggests an enhancement of AFM coupling, as predicted by the well-known BSI curve. These findings are consistent with the above restricted calculations and previous studies.[50,51] After considering magnetostructural relaxation, the FM magnetic ground state changed to the iAFM state. It should be noted, however, that the predicted trend for the electric-field control of the magnetic coupling remains consistent. Specifically, upward polarization still enhances the interlayer FM coupling by approximately 0.16 meV, while downward polarization yields a significantly stronger enhancement of the interlayer AFM coupling, at approximately 25.77 meV.

To understand the effects of polarization directions on the electronic properties of the Cr_2S_2Se/In_2Se_3 heterostructure, we calculate the projected band structure and DOS of the heterostructure with upward and downward polarizations, as shown in Figures 5 and S9 in the SI. In order to compare the valley polarizations between the Janus Cr_2S_2Se monolayer and the heterostructure, SOC for only the magnetization along the $+z$ direction is considered. When the polarization is upward, the heterostructure exhibits metallic behavior, as evidenced by two bands crossing the Fermi level around the Γ and K′ points. As shown in Figure S10 of the SI, the metallicity remains robust across different values of U, confirming that it is not an artifact of a specific parameter choice. The bands near the Fermi level mainly come from Cr and Se in the In_2Se_3 layer. After the polarization direction turns downward, the band gap reopens up and shows the semiconducting characteristics with a direct band gap of 0.67 eV. Both the band edges of the heterostructure position at the Γ point, in which the CBM and VBM mainly come from the states of In and Se in the Cr_2S_2Se layer. The upward polarization enhances the valley polarization to $|\Delta E| = 42$ meV, while the downward polarization suppresses that to $|\Delta E| = 14$ meV.

The exchange parameters and MAEs of the Cr_2S_2Se/In_2Se_3 heterostructure for both upward and downward polarizations are also calculated. The exchange parameters are $J_1 = 5.90$ $J_2 = 7.37$, and $J_3 = 0.30$ meV for upward polarization, and $J_1 = 6.90$, $J_2 = 9.20$, and $J_3 = -2.61$ meV for downward polarization, respectively. The negative J_3 for downward polarization is consistent with its iAFM ground state. Moreover, the upward polarization gives rise to an out-of-plane MAE of 188 μeV/Cr, while the downward polarization results in an in-plane MAE of 21 μeV/Cr. We also estimate the transition temperatures of the Cr_2S_2Se/In_2Se_3 heterostructure with upward and downward polarizations, as shown in Figure S11 in the SI. The transition temperatures for upward and downward polarizations are estimated to be about 251 and 356 K, respectively, indicating the possibilities of experiments and applications.

4. CONCLUSION

In conclusion, we performed systematic first-principles studies on the physical properties and electric-field manipulation of the Janus Cr_2S_2Se monolayer. The Janus Cr_2S_2Se monolayer is synthetically feasible in terms of energy, dynamical, and thermal stabilities. As a result of the strong ferromagnetic superexchange interaction, its magnetic ground state favors the ferromagnetic configuration with high Curie temperature of 279 K. It is a semiconductor with an indirect band gap of 0.44 eV. With considering spin−orbital coupling along the $\pm z$ direction, the energies of conduction band minimum at K and K′ show valley polarization with an energy difference of 33 meV. By constructing a Cr_2S_2Se/In_2Se_3 heterostructure, the spin and valley polarizations of the Janus Cr_2S_2Se monolayer can be tuned by the polarization direction. When the polarization is switched from upward to downward direction, the structural deformation and charge transfer result in the ferromagnetic-to-antiferromagnetic and metal-to-semiconductor transitions, and the valley polarization is suppressed. Our studies unveiled the structural, magnetic, and electronic properties of the Janus Cr_2S_2Se monolayer and demonstrated that, in the heterostructure, these properties can be switched

https://doi.org/10.1021/acs.jpcc.5c08067
J. Phys. Chem. C 2026, 130, 4216−4222

by controlling the polarization direction. It makes the Janus Cr_2S_2Se monolayer promising candidates for the use in next-generation low-dimensional spintronics applications.

■ ASSOCIATED CONTENT

Supporting Information

The Supporting Information is available free of charge at https://pubs.acs.org/doi/10.1021/acs.jpcc.5c08067.

Tests of computational parameters, phonon spectrum, AIMD simulation, different magnetic configurations, orbital-resolved MAEs, projected DOS, orbital-resolved band structure, spin-polarization band structure, and *x*-magnetized band structure of the Janus monolayer, as well as the controllability analyses, projected DOS, and MC simulations of the heterojunction (PDF)

■ AUTHOR INFORMATION

Corresponding Author

Yanning Zhang − *Institute of Fundamental and Frontier Sciences, University of Electronic Science and Technology of China, Chengdu 611731, China; Key Laboratory of Quantum Physics and Photonic Quantum Information (University of Electronic Science and Technology of China), Ministry of Education, Chengdu 611731, China;* orcid.org/0000-0002-3839-2965; Email: yanningz@uestc.edu.cn

Authors

Deju Zhang − *Institute of Fundamental and Frontier Sciences, University of Electronic Science and Technology of China, Chengdu 611731, China; Key Laboratory of Quantum Physics and Photonic Quantum Information (University of Electronic Science and Technology of China), Ministry of Education, Chengdu 611731, China;* orcid.org/0000-0001-6787-4245

Zhe Wang − *Department of Physics and Astronomy, University of California, Irvine, California 92697, United States*

Sihang Che − *Yingcai Honors College, University of Electronic Science and Technology of China, Chengdu 611731, China*

Wei Ji − *Institute of Fundamental and Frontier Sciences, University of Electronic Science and Technology of China, Chengdu 611731, China; Beijing Key Laboratory of Optoelectronic Functional Materials & Micro-Nano Devices, Department of Physics, Renmin University of China, Beijing 100872, China;* orcid.org/0000-0001-5249-6624

Complete contact information is available at: https://pubs.acs.org/10.1021/acs.jpcc.5c08067

Notes

The authors declare no competing financial interest.

■ REFERENCES

(1) Fiebig, M.; Lottermoser, T.; Meier, D.; Trassin, M. The evolution of multiferroics. *Nat. Rev. Mater.* **2016**, *1*, No. 16046.

(2) Kimura, T.; Goto, T.; Shintani, H.; Ishizaka, K.; Arima, T.; Tokura, Y. Magnetic control of ferroelectric polarization. *Nature* **2003**, *426*, 55−58.

(3) Xue, F.; Wang, Z.; Hou, Y.; Gu, L.; Wu, R. Control of magnetic properties of $MnBi_2Te_4$ using a van der Waals ferroelectric III_2-VI_3 film and biaxial strain. *Phys. Rev. B* **2020**, *101*, No. 184426.

(4) Cheng, H.-X.; Zhou, J.; Wang, C.; Ji, W.; Zhang, Y.-N. Nonvolatile electric field control of magnetism in bilayer CrI_3 on monolayer In_2Se_3. *Phys. Rev. B* **2021**, *104*, No. 064443.

(5) Huang, B.; Clark, G.; Navarro-Moratalla, E.; Klein, D. R.; Cheng, R.; Seyler, K. L.; Zhong, D.; Schmidgall, E.; McGuire, M. A.; Cobden, D. H.; Yao, W.; Xiao, D.; Jarillo-Herrero, P.; Xu, X. Layer-dependent ferromagnetism in a van der Waals crystal down to the monolayer limit. *Nature* **2017**, *546*, 270−273.

(6) Gong, C.; Li, L.; Li, Z.; Ji, H.; Stern, A.; Xia, Y.; Cao, T.; Bao, W.; Wang, C.; Wang, Y.; Qiu, Z. Q.; Cava, R. J.; Louie, S. G.; Xia, J.; Zhang, X. Intrinsic long-range ferromagnetic order is observed in few-layer $Cr_2Ge_2Te_6$ crystals, with a transition temperature that can be controlled using small magnetic fields. *Nature* **2017**, *546*, 265−269.

(7) Mermin, N. D.; Wagner, H. Absence of Ferromagnetism or Antiferromagnetism in One- or Two-Dimensional Isotropic Heisenberg Models. *Phys. Rev. Lett.* **1966**, *17*, No. 1133.

(8) Eerenstein, W.; Mathur, N. D.; Scott, J. F. Multiferroic and magnetoelectric materials. *Nature* **2006**, *442*, 759−765.

(9) Dong, S.; Liu, J. M.; Cheong, S. W.; Ren, Z. Multiferroic materials and magnetoelectric physics: Symmetry, entanglement, excitation, and topology. *Adv. Phys.* **2015**, *64*, 519−626.

(10) Wang, K. F.; Liu, J.-M.; Ren, Z. F. Multiferroicity: The coupling between magnetic and polarization orders. *Adv. Phys.* **2009**, *58*, 321−448.

(11) Lee, J. H.; Fang, L.; Vlahos, E.; Ke, X.; Jung, Y. W.; Kourkoutis, L. F.; Kim, J.-W.; Ryan, P. J.; Heeg, T.; Roeckerath, M.; Goian, V.; Bernhagen, M.; Uecker, R.; Hammel, P. C.; Rabe, K. M.; Kamba, S.; Schubert, J.; Freeland, J. W.; Muller, D. A.; Fennie, C. J.; Schiffer, P.; Gopalan, V.; Johnston-Halperin, E.; Schlom, D. G. A strong ferroelectric ferromagnet created by means of spin-lattice coupling. *Nature* **2010**, *466*, 954−958.

(12) Jiang, P.; Zheng, X.; Kang, L.; Tao, X.; Huang, H.-M.; Dong, X.; Li, Y.-L. $Mn_2P_2S_3Se_3$: a two-dimensional Janus room-temperature antiferromagnetic semiconductor with a large out-of-plane piezoelectricity. *J. Mater. Chem. C* **2023**, *11*, 2703−2711.

(13) Wang, P.; Zong, Y.; Liu, H.; Wen, H.; Wu, H.-B.; Xia, J.-B. Highly efficient photocatalytic water splitting and enhanced piezoelectric properties of 2D Janus group-III chalcogenides. *J. Mater. Chem. C* **2021**, *9*, 4989−4999.

(14) Guo, S.-D.; Zhu, Y.-T.; Mu, W.-Q.; Chen, X.-Q. A piezoelectric quantum spin Hall insulator with Rashba spin splitting in Janus monolayer SrAlGaSe. *J. Mater. Chem. C* **2021**, *9*, 7465−7473.

(15) Guo, S.-D.; Guo, X.-S.; Zhu, Y.-T.; Ang, Y.-S. Predicted ferromagnetic monolayer CrSCl with large vertical piezoelectric response: A first-principles study. *Appl. Phys. Lett.* **2022**, *121*, No. 062403.

(16) Guo, S.-D.; Zhu, Y.-T.; Qin, K.; Ang, Y.-S. Large out-ofplane piezoelectric response in ferromagnetic monolayer NiClI. *Appl. Phys. Lett.* **2022**, *120*, No. 232403.

(17) Guan, Z.; Luo, N.; Ni, S.; Hu, S. Tunable electronic and magnetic properties of monolayer and bilayer Janus $Cr_2Cl_3I_3$: a first-principles study. *Mater. Adv.* **2020**, *1*, 244−253.

(18) Zhang, F.; Mi, W.; Wang, X. Spin-Dependent Electronic Structure and Magnetic Anisotropy of 2D Ferromagnetic Janus $Cr_2I_3X_3$ (X = Br, Cl) Monolayers. *Adv. Elect. Mater.* **2020**, *6*, No. 1900778.

(19) Hou, Y.; Xue, F.; Qiu, L.; Wang, Z.; Wu, R. Multifunctional two-dimensional van der Waals Janus magnet Cr-based dichalcogenide halides. *npj Comput. Mater.* **2022**, *8*, No. 120.

(20) Kresse, G.; Furthmüller, J. Efficient iterative schemes for ab initio total-energy calculations using a plane-wave basis set. *Phys. Rev. B* **1996**, *54*, No. 11169.

(21) Hafner, Ju. Materials simulations using VASP—a quantum perspective to materials science. *Comput. Phys. Commun.* **2007**, *177*, 6−13.

(22) Perdew, J. P.; Burke, K.; Ernzerhof, M. Generalized Gradient Approximation Made Simple. *Phys. Rev. Lett.* **1996**, *77*, No. 3865.

(23) Parlinski, K.; Li, Z. Q.; Kawazoe, Y. First-Principles Determination of the Soft Mode in Cubic ZrO_2. *Phys. Rev. Lett.* **1997**, *78*, No. 4063.
(24) Holzwarth, N.; Tackett, A.; Matthews, G. A Projector Augmented Wave (PAW) code for electronic structure calculations, Part I: atompaw for generating atom-centered functions. *Comput. Phys. Commun.* **2001**, *135*, 329−347.
(25) Chen, J.; Guo, Y.; Ma, C.; Gong, S.; Zhao, C.; Wang, T.; Dong, X.; Jiao, Z.; Ma, S.; Xu, G.; An, Y. Magnetic Nanodevices and Spin-Transport Properties of a Two-Dimensional CrSCl Monolayer. *Phys. Rev. Appl.* **2023**, *19*, No. 054013.
(26) Mogulkoc, A.; Modarresi, M.; Rudenko, A. N. Two-dimensional chromium pnictides CrX (X = P, As, Sb): Half-metallic ferromagnets with high Curie temperature. *Phys. Rev. B* **2020**, *102*, No. 024441.
(27) Mogulkoc, A.; Modarresi, M.; Rudenko, A. N. Two-Dimensional Chromium Bismuthate: A Room-Temperature Ising Ferromagnet with Tunable Magneto-Optical Response. *Phys. Rev. Appl.* **2021**, *15*, No. 064053.
(28) Modarresi, M.; Mogulkoc, A.; Mogulkoc, Y.; Rudenko, A. N. Lateral Spin Valve Based on the Two-Dimensional CrN/P/CrN Heterostructure. *Phys. Rev. Appl.* **2019**, *11*, No. 064015.
(29) Dai, D.; Whangbo, M.-H. Spin-Hamiltonian and density functional theory descriptions of spin exchange interactions. *J. Chem. Phys.* **2001**, *114*, 2887−2893.
(30) Whangbo, M.-H.; Koo, H.-J.; Dai, D. Spin exchange interactions and magnetic structures of extended magnetic solids with localized spins: theoretical descriptions on formal, quantitative and qualitative levels. *J. Solid State Chem.* **2003**, *176*, 417−481.
(31) Xiang, H. J.; Kan, E. J.; Wei, S.-H.; Whangbo, M.-H.; Gong, X. G. Predicting the spin-lattice order of frustrated systems from first principles. *Phys. Rev. B* **2011**, *84*, No. 224429.
(32) Baroni, S.; de Gironcoli, S.; Dal Corso, A.; Giannozzi, P. Phonons and related crystal properties from density-functional perturbation theory. *Rev. Mod. Phys.* **2001**, *73*, No. 515.
(33) Togo, A.; Oba, F.; Tanaka, I. First-principles calculations of the ferroelastic transition between rutile-type and $CaCl_2$-type SiO_2 at high pressures. *Phys. Rev. B* **2008**, *78*, No. 134106.
(34) Li, Y.; Wu, Y.; Deng, L.; YIn, X.; Han, X.; Tian, F.; Zhang, X. Spontaneous spin and valley polarizations in a twodimensional Cr_2S_3 monolayer. *J. Appl. Phys.* **2023**, *133*, No. 134301.
(35) He, Z.; Peng, R.; Feng, X.; Xu, X.; Dai, Y.; Huang, B.; Ma, Y. Two-dimensional valleytronic semiconductor with spontaneous spin and valley polarization in single-layer Cr_2Se_3. *Phys. Rev. B* **2021**, *104*, No. 075105.
(36) Liu, M.; Huang, Y. L.; Gou, J.; Liang, Q.; Chua, R.; Arramel; Duan, S.; Zhang, L.; Cai, L.; Yu, X.; Zhong, D.; Zhang, W.; Wee, A. T. S. Diverse Structures and Magnetic Properties in Nonlayered Monolayer Chromium Selenide. *J. Phys. Chem. Lett.* **2021**, *12*, 7752−7760.
(37) Liu, Z.; Sun, Z.; Qu, X.; Nie, K.; Yang, Y.; Li, B. L.; Chong, S.; Yin, Z.; Huang, W. Solution-Processable Microstructuring of 1T′-Phase Janus MoSSe Monolayers for Boosted Hydrogen Production. *J. Am. Chem. Soc.* **2024**, *146*, 23252−23264.
(38) Anderson, P. W. Antiferromagnetism. Theory of Superexchange Interaction. *Phys. Rev.* **1950**, *79*, No. 350.
(39) Goodenough, J. B. An interpretation of the magnetic properties of the perovskite-type mixed crystals $La_{1-x}Sr_xCoO_{3-\lambda}$. *J. Phys. Chem. Solids* **1958**, *6*, 287−297.
(40) Kanamori, J. Superexchange interaction and symmetry properties of electron orbitals. *J. Phys. Chem. Solids* **1959**, *10*, 87−98.
(41) Azumi, K.; Goldman, J. E. Volume Magnetostriction in Nickel and the Bethe-Slater Interaction Curve. *Phys. Rev.* **1954**, *93*, No. 630.
(42) Cardias, R.; Szilva, A.; Bergman, A.; Marco, I. D.; Katsnelson, M. I.; Lichtenstein, A. I.; Kvashnin, Y. O.; et al. The Bethe-Slater curve revisited; new insights from electronic structure theory. *Sci. Rep.* **2017**, *7*, No. 4058.
(43) Qing, X.; Li, H.; Zhong, C.; Zhou, P.; Dong, Z.; Liu, J. Magnetism and spin exchange coupling in strained monolayer CrOCl. *Phys. Chem. Chem. Phys.* **2020**, *22*, 17255−17262.
(44) Gong, C.; Kim, E. M.; Wang, Y.; Lee, G.; Zhang, X. Multiferroicity in atomic van der Waals heterostructures. *Nat. Commun.* **2019**, *10*, No. 2657.
(45) Wu, Y.; Zhang, D.; Zhang, Y.-N.; Deng, L.; Peng, B. Nonreciprocal and Nonvolatile Electric-Field Switching of Magnetism in van der Waals Heterostructure Multiferroics. *Nano Lett.* **2024**, *24*, 5929−5936.
(46) Eom, J.; Lee, I. H.; Kee, J. Y.; Cho, M.; Seo, J.; Suh, H.; Choi, H.-J.; Sim, Y.; Chen, S.; Chang, H. J.; Baek, S.-H.; Petrovic, C.; Ryu, H.; Jang, C.; Kim, Y. D.; Yang, C.-H.; Seong, M.-J.; Lee, J. H.; Park, S. Y.; Choi, J. W. Voltage control of magnetism in $Fe_{3-x}GeTe_2/In_2Se_3$ van der Waals ferromagnetic/ferroelectric heterostructures. *Nat. Commun.* **2023**, *14*, No. 5605.
(47) Troeye, B. V.; Lherbier, A.; Charlier, J.-C.; Gonze, X. Large phosphorene in-plane contraction induced by interlayer interactions in graphene-phosphorene heterostructures. *Phys. Rev. Mater.* **2018**, *2*, No. 074001.
(48) Muroni, A.; Brozzesi, S.; Bechstedt, F.; Gori, P.; Pulci, O. Tuning Gaps and Schottky Contacts of Graphene/Phosphorene Heterostructures by Vertical Electric Field and Strain. *Nanomaterials* **2023**, *13*, No. 2358.
(49) Wang, C.; Zhou, X.; Pan, Y.; Qiao, J.; Kong, X.; Kaun, C.-C.; Ji, W. Layer and doping tunable ferromagnetic order in two-dimensional CrS_2 layers. *Phys. Rev. B* **2018**, *97*, No. 245409.
(50) Zhang, D.; Yang, Z.; Wu, T.; Ji, W.; Zhang, Y. Switchable magnetic and electronic properties in CrSX (X = Cl, Br, I) monolayers. *Phys. Rev. Mater.* **2025**, *9*, No. 054004.
(51) Zhang, D.; Zhang, Y. Strain-selected magnetic ordering in 1T'a-CrXY (X, Y = S, Se, Te) monolayers. *Phys. Chem. Chem. Phys.* **2026**, *28*, 953−959.

https://doi.org/10.1021/acs.jpcc.5c08067
J. Phys. Chem. C 2026, 130, 4216−4222